# ENTRY, DESCENT AND IMPACT SYSTEM DESIGN AND ANALYSIS OF A SMALL PLATFORM IN MARTIAN ENVIRONMENT

IAC-20, D1,4B, 8, x59240

# ENTRY, DESCENT AND IMPACT SYSTEM DESIGN AND ANALYSIS OF A SMALL PLATFORM IN MARTIAN ENVIRONMENT

**Daniele Calvi[a]*, Fabrizio Stesina[b], Prof. Sabrina Corpino[c]**

[a] *Department of Mechanical and Aerospace engineering, Politecnico di Torino, Corso duca degli abruzzi, 10129 Torino, Italy*, daniele.calvi@polito.it
[b] *Department of Mechanical and Aerospace engineering, Politecnico di Torino, Corso duca degli abruzzi, 10129 Torino, Italy*, fabrizio.stesina@polito.it
[c] *Department of Mechanical and Aerospace engineering, Politecnico di Torino, Corso duca degli abruzzi, 10129 Torino, Italy*, sabrina.corpino@polito.it
* Corresponding Author

**Abstract**

Thanks to the latest Mars missions, planetary exploration has made enormous strides over the past ten years increasing the interest of the scientific community and beyond. These missions must fulfil many complex operations which are of paramount importance to mission success. Among these, a special mention goes to the Entry, Descent and Landing (EDL) functions which require a dedicated system to overcome all the obstacles of these critical phases. The goal of this study is to describe in detail the design methodology for EDL system during the preliminary phase of the design. The design is supported by a simulation tool integrating the entry trajectory algorithm. The trajectory data computed are used to size the EDL system and strategy in order to have a low aerodynamic acceleration, low dynamic pressure and low convective heat flux incoming to the spacecraft. The reference mission has the goal to find bioevidence and biohazards on Martian subsurface in order to prepare future manned missions. The mission is based on Space Penetrator Systems (SPS) that can descend on Mars surface following a ballistic fall and penetrate the ground after the impact with the surface (around 50 and 300 cm depth). The SPS contains all the instrumentation required to sample and make the required analyses. As results, an Entry Descent and Impact (EDI) system based on inflatable structure is designed, respecting the low-cost and low-mass constraints. For this mission, a solution, like the one of Finnish Meteorological Institute in the Mars Met-Net mission, is chosen, using an inflatable Thermal Protection System (TPS) called Inflatable Braking Unit (IBU) and an additional inflatable decelerator. Consequently, there are three configurations during the EDI phases: at an altitude of 125 km, the IBU is inflated at speed 5.5 km/s; at an altitude of 16 km, the IBU is jettisoned and an Additional Inflatable Braking Unit (AIBU) is inflated; at last, at about 13 km, the SPS is ejected from AIBU and it impacts on the Martian surface. In this paper, the results obtained by the application of this design methodology are presented and, the obtained system and descent strategy satisfy the requirements of the mission.

**Keywords: Space Penetrator System, Impact, Landing, Mars, small platform**

**Nomenclature**

| | | | |
|---|---|---|---|
| m | Mass | c | Speed of sound |
| $\dot{Q}$ | Heat flux | D | Drag |
| L | Lift | $C_d$ | Drag coefficient |
| q | Dynamic pressure | $k$ | Heat-transfer coefficient |
| V | Velocity | $\rho$ | Density |
| $R_p$ | Planet radius | R | Gas constant |
| h | Altitude | $r_n$ | Nose radius |
| r | $R_p$+h | T | Temperature |
| g | Acceleration of gravity | H | Scale height |
| $\gamma$ | Flight Path angle | $\gamma$ | Ratio of specific heats |
| $\sigma$ | Bank angle | p | Static pressure |
| n | Number of g's | $D_p$ | Penetration depth |
| λ | Longitude | Z | Soil number |
| φ | Latitude | N | Nose performance coefficient |
| ψ | Heading angle | $F_c$ | Conservative force |
| ω | Angular velocity of the planet | $F_{nc}$ | Non conservative force |
| M | Mach number | E | Kinetic energy |
| | | U | Potential energy |

| | |
|---|---|
| β | Ballistic coefficient |
| S | Cross area |

**Acronyms/Abbreviations**

| | |
|---|---|
| **AIBU** | Additional Inflatable Braking Unit |
| **D.A** | Drag Area |
| **DOF** | Degree Of Freedom |
| **EDI** | Entry, Descent and Impact |
| **EDL** | Entry, Descent and Landing |
| **FEA** | Finite Element Analysis |
| **FEM** | Finite Element Method |
| **FMI** | Finnish Meteorological Institute |
| **FPA** | Flight Path Angle |
| **IBU** | Inflatable Braking Unit |
| **LVLH** | Local Vertical-Local Horizontal frame |
| **MEPAG** | Mars Exploration Program Analysis Group |
| **SPS** | Space Penetrator System |
| **SRB** | Solid Rocket Booster |
| **MarCO** | Mars Cube One |
| **SALUS-1** | Spacecraft to Analyze Life-evidences Underneath Soil |
| **LOP-G** | Lunar Orbital Platform-Gateway |
| **TPS** | Thermal Protection System |

## 1. Introduction

Nowadays, the small platforms have attracted the attention of not only the research and academic communities, but also to space industry, agencies for their capabilities of low cost and fast delivery.

Thanks to the development of the miniaturisation of the technologies, micro- and nanosatellites represent disruptive solutions that can change the way to approach the space.

While a few years ago these kind of spacecraft have been considered only for Low-Earth Orbit mission, with the success of MarCO mission [1], a new era of space exploration has begun, expanding the potential of the space missions they can accomplish. For example, they can be used in support to space station, like the future Lunar Orbital Platform-Gateway (LOP-G) as described in the paper [2],or to monitor the space weather [3] or for scientific purposes, like astrobiology as reported in [4].

In addition, nowadays, the small platforms able to land on the planetary surface are interesting concepts waiting to be developed in spacecraft ready to launch.
In [5], the University of Arizona proposed to develop a Lunar CubeSat Lander (27U) that will be deployed from the Lunar Gateway Logistics Module (presumed to be at L2) to perform science and exploration of the lunar surface. Other interesting concepts have been developed by Politecnico di Torino in [6], proposing a mission with small platforms to serve astrobiology goals and support to future human exploration on Mars. Non-conventional solution has been reported by Finnish Meteorological Institute (FMI) and EADS Astrium using a Space Penetrator. FMI with the mission METNET [7] proposed a penetrator to investigate on global and related local phenomena on Mars such as atmospheric circulation patterns, boundary layer phenomena, water, dust and climatological cycles. The space penetrator system of ASTRIUM has been developed in order to impact the Europa surface to perform astrobiological, chemistry and geophysics experiments [8].
These missions imply to fulfil many complex operations which are of paramount importance to mission success.

Among these phases, a special mention goes to the Entry, Descent and Landing (EDL) functions which require a dedicated system to overcome all the obstacles of these critical phases.

For this reason, the study presented in this paper aims to present a methodology to design the entry, descent and landing system and strategy. In Support to this methodology, a tool integrating entry trajectory has been developed and it has been reported in this work.

This methodology and tool have been used to study the feasibility of a mission developed by Politecnico di Torino and reported in [6].

The study presented in this article has been conducted starting from the description of the reference mission, which aims to find bio-evidence and bio-hazard in order to support the future manned missions using a Space Penetrator System that analyses the soil composition under about 3 meters of depth thanks to the impact force due to kinetic energy.

Section 2 describes the process followed for the design of the entry and descent system for a preliminary study. Main design drivers and constraints are listed, basing on past Martian missions. Section 3 gives an overview of the theory on which the tool is based, reporting the equations and the assumptions used in this work.

Section 4 presents the results computing for this case study using the methodology and tool reported in section 3.

Finally, Section 5 concludes the paper with discussion of the results obtained so far, and the future steps.

### *1.1. Reference mission: SALUS-1*

The goals of this mission were proposed by MEPAG [9] that is a community-based forum designed to provide science input from the scientific community to NASA, for the planning and prioritization of Mars future exploration activities, and to facilitate for the Mars

Exploration Program. One of MEPAG's primary products is the "Mars Science Goals, Objectives, Investigations, and Priorities", which is regularly updated by the Goal Committee to reflect the current state of knowledge, plans, and inquiry about Mars with regards to life, climate, Geology and human exploration. In this document four goals are proposed:

1. Determine if life ever arose on Mars;
2. Understanding the processes and history of climate on Mars;
3. Determine the evolution of the surface and interior on Mars;
4. Prepare for human Mars exploration.

The Goal 4 is different in nature from the former three, commonly referred to as Life, Climate, and Geology. Unlike Goals 1-3, which focus on answering scientific questions to develop a comprehensive understanding of Mars as a system, Goal IV addresses issues that have relatively specific metrics related to increasing safety, decreasing risk and cost, and increasing the performance of the first crewed mission to the planet.

Focusing on the GOAL 4, in order to prepare the human exploration of Mars it is necessary to fill the gaps in the knowledge in, and to address the uncertainties related to specific phenomena in the Mars' environment (orbit, atmosphere, ground).

The reference mission (patch in the Figure 1), named Spacecraft to Analyze Life-evidences Underneath Soil (SALUS-1), aims to fill these gaps in knowledge, focusing to search bio-evidences or bio-hazards on Mars, as suggested in the following scientific goal:

*"Searching for evidences on Martian (sub) surface that could represent hazard for human exploration, together with understanding if past/present life existed/exists on Mars."*

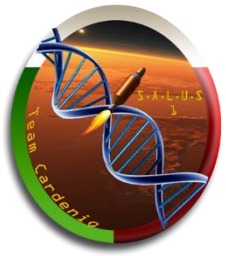


Figure 1: Patch of SALUS-1 mission

The team gathered the information needed to understand what, where and how to find these evidences. The most important organic compounds turned out to be the amino acids because they could potentially represent the "base of life". These biomarkers can be found through some optical analysis methods like Raman Spectroscopy, the Infrared Spectroscopy, UV Fluorescence, and Capillary Electrophoresis (Mars Organic Analyzer).

In order to sample and analyse the Martian soil, three candidate methods for soil penetration methods were assessed: laser, drill, and impact. As the penetration methods are concerned, the drilling involves different techniques: force, heat, chemical reactions, and ultrasonic waves. In any case a CubeSat size system was considered unlikely to provide sufficient force or energy for these solutions. The impact solution with the Space Penetrator System instead seemed very promising at the first glance. Though there have not been successful planetary penetrator missions yet, three systems have been developed and tested on the ground: Deep Space-2 (DS-2), Mars'96 and Lunar-A. Moreover, a lot of work has been done in this field and a great number of new concepts have been developed in the last years. An interesting one is developed by the old EADS Astrium for mission on the Jovian moon EUROPA, and the Space Penetrator System (SPS) will contain all the instrumentation required to sample and make the required analyses. During the test, successfully completed, the penetrator experienced a deceleration of 24000 g [8]. Such a system can be deployed from carrier, it is designed for hard landing, breaking through ice and regolith (soil) and penetrating to 2-3m depth; instruments might include sample retrieval drill, optical microscope and mass spectrometer (Figure 2).

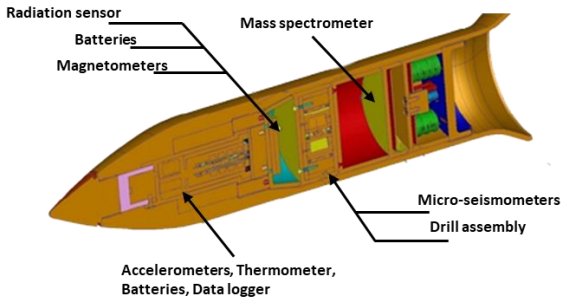


Figure 2: SPS configuration [8]

Since the presence of the atmosphere and the high speed reached during the entry and descent, the SPS shall be supported by an EDI system in order to withstand to the high temperature and to reduce the speed until the impact. For this reason, a solution proposed by FMI for the mission METNET is chosen and the design reference mission has been reported in the Figure 3.

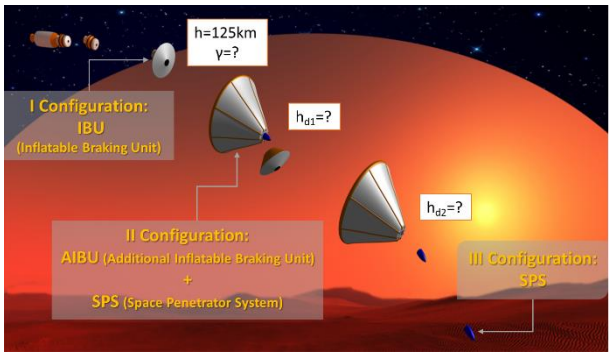

Figure 3: Design Reference Mission of SALUS-1

Taking into account from the figure above, during the EDI phase, three configurations have been defined:

1. I configuration: the Inflatable braking Unit (IBU) will be inflated at an altitude of 125 km in order to protect the SPS against the high heat flux during the hypersonic flight.
2. II configuration: At the altitude $h_{d1}$, an additional inflatable braking unit (AIBU) will be inflated to decelerate the descent and, at the same time, the IBU will be ejected.
3. III configuration: At an altitude of $h_{d2}$ the SPS will separate from AIBU and will impact the Martian soil.

As can be seen in the Figure 3, the flight path angle (FPA) $\gamma$, $h_{d1}$, $h_{d2}$ are unknown and they can be computed thanks to the tool described in the next section.

## 2. Methodology & Tool

In this section, the methodology and tool to design the system and strategy have been reported.

For the design of the geometry of the IBU and AIBU, some constraints have been considered taking into account past Martian mission and new concepts. With the geometrical parameters, also the information about strategy, like flight path angles and the altitude to deploy the inflatable structures, are iterated with the support of a simulation tool integrating the entry trajectory algorithm.

In the Figure 4 the methodology flow chart has been reported.

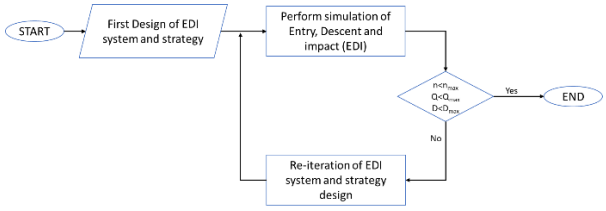

Figure 4: Methodology flow chart

The methodology has been supported by a simulation tool compiled in MATLAB, exploiting the equation and the theory reported in the next section.

The flow chart of the tool is summarised in the Figure 5. Once setting the input regarded the entry vehicle data, like geometry and aerodynamic database, and planetary data, like atmospheric model and physical parameters, the position and velocity data are integrated with an assumption regarded the attitude in which a ballistic fall is considered. When the impact is come, the penetration depth is computed with a semi-empiric formula that considers the soil properties, and then number of gees due to the impact is computed considering that all the kinetic energy has been transformed into "impact energy".

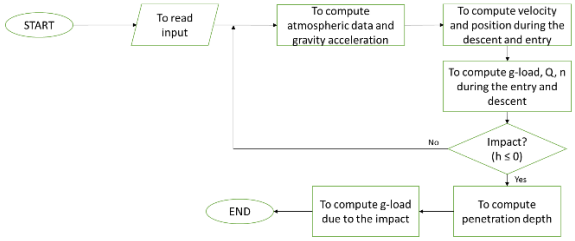

Figure 5: Tool flow chart

### *2.1. Design consideration*

Regarding the geometry of the inflatable structures for the entry and descent and mass budget of the entry vehicle, some considerations have been made considering past missions.

MASS BUDGET

To perform a mass budget, some statistical considerations have been done. In this preliminary analysis is suggested to overestimate the mass. For this reason, the IBU mass has been estimated considering the conventional rigid TPS.

The total mass is composed by the following three contributes:

$$m_{tot} = m_{payload+subsys} + m_{AIBU} + m_{IBU}$$

Taking into account statistical data present in literature, the mass of the TPS frontal part can be assigned considering the maximum dynamic pressure. Moreover, using the chart reported in the Figure 6, it is possible to obtain a relation between the peak dynamic pressure and the frontal TPS structural mass fraction.

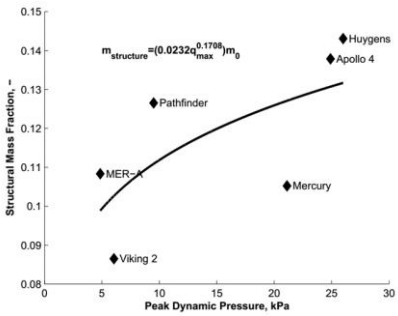

Figure 6:Trend of the Structural Mass Fraction of the Frontal part of the TPS

Regarding the rear part, it is usually:

$$m_{rTPS} = 0.14 \cdot m_{tot}$$

Thus, the IBU mass is:

$$m_{IBU} = m_{rTPS} + m_{fTPS}$$

For the $m_{payload+subsys}$, it is considered that it is equal to the 60% of the total system mass.

In order to overestimate, the $m_{tot}$ is assumed to be 80 kg and $q_{max}$ is assumed to be 10 kPa and the results of the mass budget are reported in the Table 1.

Table 1: Mass budget for the three configuration

| | |
|---|---|
| $m_{SPS}$ | 48 kg |
| $m_{IBU}$ | 20.15 kg |
| $m_{AIBU}$ | 11.85 kg |

IBU

For the IBU, Super light-weight ablative material has been chosen because it has been used also in past Martian missions. With this consideration, it is possible to define the constraint regarded the maximum heat flux during the entry of 300 W/cm$^2$ [10].

A shape based on BEAGLE2 configuration has been considered because it is similar to the IBU shape of MetNet.

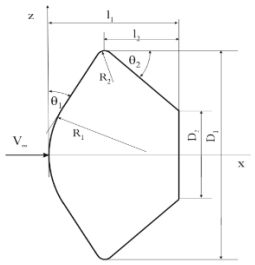


Figure 7:Shape of Beagle-2 heat shield [10]

Tacking into account the same geometrical characteristic of the shape, it is possible to compute the geometric parametric indicated in the Figure 7 and reported in the Table 2.

Table 2: Geometrical parameters for IBU

| | |
|---|---|
| **$D_2$** | 0.55 m |
| **$D_1$** | 1.33 m |
| **$l_1$** | 0.65 m |
| **$l_2$** | 0.40 m |
| **$th_{inside}$** | 0.60 m |
| **$th_{frontal}$** | 0.05 m |
| **$R_1$** | 0.33 m |

AIBU

For sizing the AIBU, the following considerations must be taken into account:

- the AIBU shall be inflated when the Mach number is less than 3 [7]
- The AIBU must be decelerate the SPS in order to have a penetration depth of 0.3÷3 m [8]

In this work the instant jettisoned and no-interference assumptions have been considered.

However, with appropriate modifications, the simulator can be used in order to estimate the AIBU geometry. Firstly, the algorithm computes the trajectory and increases the Drag Area (D.A) of the decelerator, i.e. the multiplication between drag coefficient ($C_d$) of the second configuration and $S_{ref}$ of the AIBU, until the penetration depth is acceptable. Regarding the shape of the second configuration, it is assumed similar to a cone with semi-cone angle of 37 degree in order to find the cross area with a mean value of drag coefficient during the descent.

## 3. Theory and calculation

In this section, the theory, on which the simulation tool has been developed, has been reported. The following topics have been discussed:

1. Entry corridor
2. Thermal phenomena
3. Equation of motion
4. Atmospheric model
5. Reference planet model
6. Penetration equation

### *3.1. Entry corridor*

To entry and land on a planet safely, the following conditions must be met:

- the vehicle must not burn;
- the trajectory must ensure descent;
- aerodynamic load limits must not be exceeded.

These constraints depend strictly on the vehicle type, and initial conditions. Then before carrying out an entry manoeuvre, a "corridor" must be defined:

"The entry corridor is the three-dimensional space along which a spacecraft must travel in order to pass safely through the atmosphere and achieve a successful landing."

Thus, once atmospheric contact is established, three cases exist:

- the body may skip out of the atmosphere and return to space;
- the body can be destroyed due to the action of atmospheric drag and due to the heat generated during the hypersonic descent;
- the body may traverse through the atmospheric layer to reach the planet surface.

In practice, the body could reach the surface if its flight path angle is within a tight range of values and the borderline case define the entry corridor. The Figure 8 illustrates the entry corridor concept, where two boundaries are represented:

- Overshoot boundary: if the trajectory is above this limit, the drag is too low, and the body will return to space;
- Undershoot boundary: if the trajectory is below this limit, the heat flux and the acceleration are too high and the structure of the entry vehicle would not withstand.

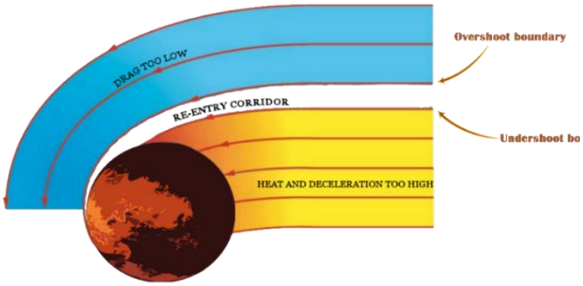


Figure 8: Entry-corridor

Therefore, for a safe entry it is necessary to consider:
- the maximum convective heat flux
- the maximum aerodynamic acceleration
- the maximum dynamic pressure
- the equilibrium glide condition

$$\dot{Q} \leq \dot{Q}_{max} \quad (1)$$

$$\frac{\left\|\vec{L}+\vec{D}\right\|}{mg} \leq n_{max} \quad (2)$$

$$q \leq q_{max} \quad (3)$$

$$\left(\frac{V^2}{r}-g\right)\cos\gamma+\frac{L}{m}\cos\sigma \leq 0 \quad (4)$$

where $\dot{Q}$ is the heat flux, g is the planet gravitational acceleration, n is the number of g-loads, q is the dynamic pressure and m is the body mass.

Regarding equation (1), $\dot{Q}\_max$ can be deduced from the Shutton-Graves equation that is an approximate expression for convective heating at stagnation point in a hypersonic flow. The constrains described in (2) and (3) depend on the vehicle structure or on the presence of humans on-board.

The last condition (4) is the equilibrium glide condition, which is related to the Bank angle (σ). This condition is not a hard constraint; it is necessary to reduce the phugoid oscillations, being more meaningful at higher altitudes.

### *3.2. Thermal Phenomena*

The convective heat flux at the stagnation point is an important parameter to find the entry trajectory.

The stagnation-region [11] flow field is characterized by a severe thermal environment, which is generated by the deceleration of a high-speed flow as it approaches the vehicle surface. The kinetic energy of the flow is converted into internal energy of the gas, with a consequent temperature increase, vibrational energy excitation and chemical reactions occurrence. In some conditions, gas ionization and radiation effects may also be present. Surface heating is the most critical aspect as far as the stagnation region is concerned.

To the purpose of this work, only this region has been analysed using the correlation reported in a simpler form by Sutton and Graves [11]. It is possible to say that the convective heat-flux is proportional to

$$\dot{Q} \propto V^{3.05}\rho^{0.5}r_n^{-0.5} \quad (5)$$

where $r_n$ is the capsule nose radius. Then, introducing the heat-transfer coefficient "k", it is possible to obtain the next equation:

$$\dot{Q}_{conv} = k\,V^{3.05}\sqrt{\frac{\rho}{r_n}} \quad (6)$$

For this relation, the assumptions are the following:
- The body is an axial symmetric blunt body
- The model considers that the gas mixtures, encountered during high velocity planetary entry, are in the chemical equilibrium.

For a general gas mixture, k is function of the molecular mass fraction and of the individual transport properties. The value for Mars is listed below:

$$k_{mars} = 1.9027\cdot 10^{-4}\,\frac{kg^{1/2}}{m}$$

Velocity, density and nose radius are expressed in SI units, therefore the heat flux is expressed in $W/m^2$.

### *3.3. Equation of motion*

An entry vehicle flies in a flight envelope that range from low-speed at low altitude up to suborbital and close-to-orbital velocities at very high altitude. In presence of an atmosphere this may result in subsonic, supersonic, or hypersonic flow regimes, in a rarefied gas at very high altitude or a dense one close to the planet surface. For this reason, the equations of motion usually adopted for describing the flight of vehicles in the atmosphere may not be suitable to describe the entire trajectory, as these equations are derived under the simplifying assumptions of flight over a flat, non-rotating planet. In this section, the equations of motion will be derived in the most general framework of flight over a spherical, rotating planet with an atmosphere.

Moreover, no propulsive and no varying mass system is considered to simulate the entry trajectories in 3 Degree of Freedom (DoF). The state vector of the motion of vehicle includes three components of position vector in rotating planetocentic frame and three component of velocity vector in Local Vertical-Local Horizontal Frame (LVLH).

In this work, the attitude equations were not considered. This is a good assumption because allows to

decouple the translational motion and rotational motion because, as discussed in [12] the translational motion is mostly associated to long-period trajectory dynamics, whereas the rotational motion is associated to short-period oscillations. Most guidance approaches consider only translational point-mass trajectory dynamics, while the short period oscillations are addressed by inner-loop attitude control algorithms.

Therefore, the state vector is:

$$s = [h\ \lambda\ \varphi\ v\ \gamma\ \psi]^T$$

and the equations of motion are:

$$\dot{r} = \dot{h} = v\sin(\gamma) \tag{7}$$

$$\dot{\lambda} = \frac{v\cos(\gamma)\ \sin(\psi)}{r\cos(\varphi)}; \tag{8}$$

$$\dot{\varphi} = \frac{v}{r}\cos(\gamma)\cos(\psi)\,; \tag{9}$$

$$\dot{v} = -\frac{D}{m} - g\sin(\gamma) + \omega^2 r\,cos(\varphi)\,(\cos(\varphi)\sin(\gamma) - \cos(\gamma)\cos(\psi)\sin(\varphi)\,); \tag{10}$$

$$v\dot{\gamma} = \frac{L}{m}\cos\sigma - \left(\frac{V^2}{r} - g\right)\cos\gamma + 2\omega v\cos(\varphi)\sin(\psi) + \omega^2 r\,cos(\varphi)\,(\cos(\varphi)\cos(\gamma) + \sin(\gamma)\cos(\psi)\sin(\varphi)\,); \tag{11}$$

$$v\dot{\psi} = -\frac{L}{m}\frac{\sin\sigma}{\cos(\gamma)} + \frac{v^2}{r}\cos\gamma\sin(\psi)\tan(\gamma) + \frac{\omega^2 r}{\cos\gamma}\cos(\varphi)\sin(\varphi)\sin(\psi) + 2\omega v(\sin(\varphi) - \cos(\varphi)\cos(\psi)\tan(\gamma)); \tag{12}$$

Where:

- r=Rp+h (Rp is planet radius and h is altitude);
- λ is longitude;
- φ is latitude;
- v is the entry vehicle velocity norm (ground speed);
- γ is the FPA and it's the angle between the velocity vector and horizontal;
- ψ is the heading angle that is defined as the angle between the local meridian and the projective of the velocity vector on the local horizontal plane.
- g is the gravitational acceleration and it range with the altitude as

$$g = g_0\left(\frac{R_p}{r}\right)^2 \tag{13}$$

In order to solve these equations, the entry vehicle aerodynamic database is useful to determinate the Drag and Lift coefficients, which are function of the Mach Number M and Angle of Attack α. This last angle is determined usually by the guidance and control functions and the Mach number relation is dependent on the RV velocity and atmospheric sound speed:

$$M = \frac{V_{RV}}{c(h)} \tag{14}$$

The speed of sound is closely related to the altitude *h* because it is function of the temperature and, consequently, of the pressure and the density of the fluid surrounding the spacecraft:

$$c = \sqrt{\gamma RT} = \sqrt{\gamma\frac{p}{\rho}} \tag{15}$$

Where:

- γ is the ratio of specific heats;
- R is the gas costant from the equation of state;
- T, p, ρ are temperature, pressure and density of the gas mixture that are function of the altitude.

There would also be the sideslip angle that could generate the side force but, in this work, it is assumed to be equal to zero.

### *3.4. Atmospheric model*

Among the forces applied to a spacecraft during its flight, the aerodynamic forces play a significant role in the dynamical behaviour of the spacecraft [13]. These forces depend on the local atmosphere properties. In the nature, the state of atmosphere varies with altitude, geographical latitude, season and time.

However, the spherical planet assumption simplifies the model. Thus, the trajectory study is predicted with the help of a model of atmosphere which uses an exponential equation to find the atmosphere density as a function of height:

$$\rho(h) = \rho_0 e^{-\frac{h}{H}} \tag{16}$$

Where $\rho_0$ is the atmospheric density at h = 0 and H is the atmospheric scale height. This last one is the increase in altitude for which the atmospheric pressure and density decrease by a factor of *e*, and it is:

$$H = \frac{RT}{g} \tag{17}$$

Since the atmosphere has some layers, each layers is identified by a scale height. In order to implement the atmospheric model, it has been considered that one scale height was sufficient to describe Mars air density; in fact, its atmosphere is very thin.

By comparison with the NASA data it is possible to see Figure 9 that this results to be a good assumption:

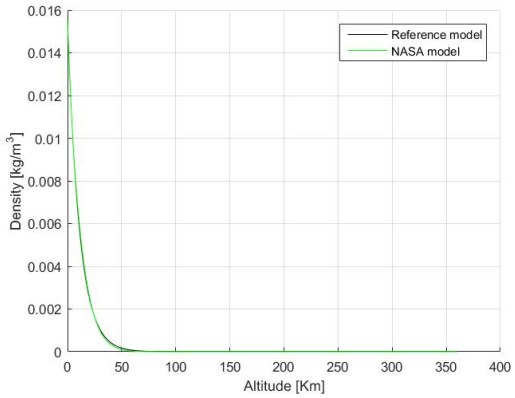


Figure 9: Martian density trends: Reference model Vs NASA model

Consequently, the used scale height is:

$$H = 11.3\ km$$

Regarding the temperature, two different models have been used.

If the altitude is higher than 50 km the used model is based on the graph reported in Figure 9. Until 50 km, the considered model is the NASA one, which has been reported in Figure 10.

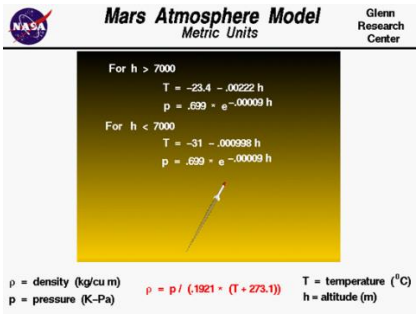


Figure 10: Mars Atmophere model [14]

Thus, the temperature profile considered in the simulation is that reported in Figure 11.

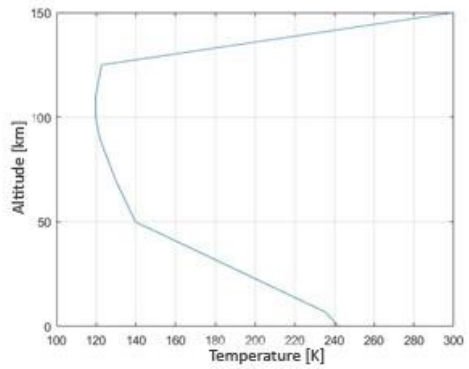


Figure 11: Temperature trends along altitude

As it can be seen from the figure above, at 125 km the temperature goes up increasing with the altitude due to the Sun energy. Above this mentioned altitude the density has little effect on the body; for this reason, this has been conventionally considered as the atmospheric altitude interface.

### *3.5. Reference planet model*

As it has been previously explained, thanks to the spherical planet assumption not many parameters are necessary in order to model the planet. In particular, the required data are those listed below.

Table 3: Planet data

| | | |
|---|---|---|
| Planet Radius ($R_p$) | 3402.4 | km |
| Standard gravitational parameter ($\mu_p$) | 42811.395 | $Km^3/s^2$ |
| Rotational angular velocity of planets ($\omega_p$) | $7.088191 \cdot 10^{-05}$ | Rad/s |
| Acceleration of Gravity on surface ($g_0$) | 3.69 | $m/s^2$ |
| Atmospheric density on surface ($\rho_p$) | 0.0150 | $Kg/m^3$ |

### *3.6. Penetration equation*

Thanks to the values of impact velocity, it is possible to obtain the penetration depth, which is an important information for the Penetrators. In order to calculate accurately the penetration depth, an analysis with Finite Element Method (FEM) needs to be done [15].

However, in this preliminary design, some semi-empirical equations have been used [16]. The following assumptions and limitations have been applied to the penetration equations:

- The penetrator remains intact during penetration
- The penetrator follows a basically stable trajectory
- The impact velocity is less than 1220 m/s
- The equations are not valid for water or air penetration
- The equations are not applicable to armor penetration (e.g. not for metals, ceramics or materials different from those listed)
- Minimum penetrator weight: about 5 pounds for soil and 10 pounds for rock, concrete, ice and frozen soil.

In this work, the equations related to Ice and to Froze Soil have been used in SI Units.

For $V_f$ <61m/s

$$D_p = 0.00024\, Z\, N \left(\frac{m}{S_{ref}}\right)^{0.6} \ln\left(1 + 2.15\, V_f^2\, 10^{-4}\right) \ln(50 + 0.29\, m^2)\,; \quad (18)$$

For $V_f \geq 61$ m/s

$$D_p = 0.0000046\, Z\, N \left(\frac{m}{S_{ref}}\right)^{0.6} \left(V_f - 30.5\right) \ln(50 + 0.29\, m^2)\,; \quad (19)$$

Where

- $D_p$ is penetration depth [m];
- Z is the Soil-number for Ice/Frozen Soil;
- N is the Nose performance Coefficient;
- Vf is the impact speed [m/s].

Regarding Z, both, freshwater ice and sea ice, will normally have an S-number of 4.5 ± 0.25. Completely frozen saturated soil will have an S-number of 2.75 ± 0.5. The S-number of partially frozen soil may be as high as 7.0, but the transition from partially frozen to unfrozen soil is not well defined.

N depends on the geometry of the length of penetrator nose (Ln) and one can be obtained it thanks to the following equations.

For tangent ogive nose shapes (Figure 12):

$$N = 0.18\, \frac{L_n}{d} + 0.56 \quad (20)$$

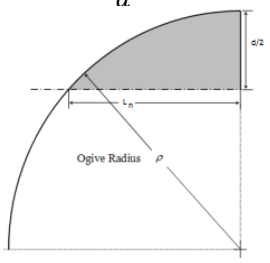


Figure 12: Tangent ogive nose shape

For conic nose shapes (Figure 13):

$$N = 0.25\, \frac{L_n}{d} + 0.56 \quad (21)$$

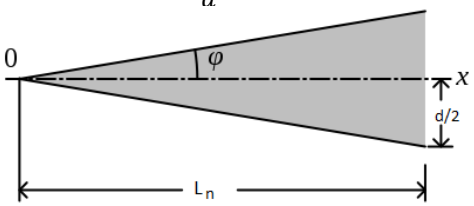


Figure 13: conic nose shapes

Once the penetration depth has been computed, the g-loads related to the impact and the impact force can be evaluated.

When the forces act on a body, the global work done by all forces must to be equal to zero. Therefore:

$$\sum \int \vec{F}_i \cdot d\vec{r}_i = \Delta E \quad (22)$$

Where:

- $F_i$ and $r_i$ are the *i-th* force acting on the body and *i-th* displacement
- E is the kinetic energy

Therefore, the force can be divided in conservative ($F_c$) and non-conservative ($F_{nc}$) force. Thus, if U is the potential energy of conservative force then the work due to non-conservative force will be:

$$\sum \int \vec{F}_{nci} \cdot d\vec{r}_i = \Delta(E + U) \quad (23)$$

Considering that all the kinetic energy has been transformed into "impact energy" (product between penetration depth and impact force) and a constant impact force, the impact force can be written:

$$F_{impact} = \frac{\frac{1}{2} m {v_f}^2}{D} \quad (24)$$

Finally, the g-load due to impact is defined as the ratio impact force and weight of the penetrator:

$$n_g = \frac{F_{impact}}{mg} \quad (25)$$

## 4. Results and discussion

Since the IBU geometry and shape has been defined, entry corridor and the geometrical parameters of the AIBU shall be defined. At the end of this section, trajectory and penetration data due to the impact are reported.

### *4.1. AIBU geometry*

As suggested in the section 2, the cross area of the AIBU has been computed, within the simulation tool, iterating the Drag Area that is the product between cross area and drag coefficient. First of all, the altitude to inflate the AIBU has been define considering that at that altitude, Mach number shall be less than 3. Setting the simulation tool with the geometrical properties of only IBU and mass of whole system, the velocity profile along the entry and descent has been computed and reported in the Figure 14.

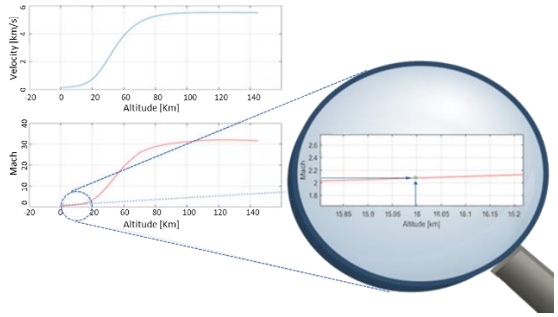


Figure 14:Velocity profile during the entry and descent

As can be seen in the figure above, the entry vehicle reaches the velocity of Mach about 2 at altitude equal to 16 km.

Setting this value as the altitude when the AIBU is inflated and IBU is ejected, $h_{d1}$, the altitude $h_{d2}$ has been computed in order to have a suitable drag area. For this

preliminary study, a drag area equal to 5 $m^2$ results to be a good compromise. From the iterations performed by the simulation tool, $h_{d2}$ results to be about 13 km to have drag area equal to 5 $m^2$. Considering, during the descent, a mean $C_d$ of the second configuration of 0.85, the cross-area results to be 5.95 $m^2$.

### *4.2. Entry corridor*

With the information about the AIBU geometry and descent strategy, in the following table, the input for simulation tool are reported.

Table 4: Input for the simulation tool

| # configurations | 3 |
|---|---|
| $m_{Iconf}$ | 80 Kg |
| $m_{IIconf}$ | 54.52 Kg |
| $m_{sps}$ | 40 Kg |
| $\beta_{Iconf}$ | 38.83 Kg/$m^2$ |
| $\beta_{IIconf}$ | 10.90 Kg/$m^2$ |
| $\beta_{sps}$ | 2123 Kg/$m^2$ |
| $S_{IBU}$ | 1.39 $m^2$ |
| $S_{AIBU}$ | 5.95 $m^2$ |
| $S_{SPS}$ | 0.0314 $m^2$ |
| $R_{nIBU}$ | 0.33 m |
| $R_{nSPS}$ | 0.01 m |
| $h_{d1}$ | 16 Km |
| $h_{d2}$ | 13.3 Km |

The undershoot boundary is define thanks to the equations explained in the section 3.1 tacking into account the following constraints:

- $Q_{max}$=300 W/$cm^2$
- $q_{max}$=10 kPa;
- $n_{max}$ is about 40g for inflatable system and 24000g for the SPS.

Keeping constant entry velocity (5.5 km/s), the FPA could be varied in order to find:

- The maximum FPA (in absolute value): above this value, the Speed profile intersects the trends of the undershoot boundary. In this case, this FPA results to be -8.2 deg.
- The minimum FPA (in absolute value): below this value, the trajectory does not continue the descent and the probe does not reach the surface (bouncing with the atmosphere). In this case, the overshoot boundary results to be FPA=-30 deg.

### *4.3. Trajectory*

Once defined the FPA that respects the constraints imposed by entry corridor, it is possible to obtain the data of trajectory and penetration depth. For this case study, a FPA equal to -13deg is considered also because it is similar to the one chosen by past Martian mission.

This choice is supported by trends altitude/range (Figure 15), in which the trajectory with the FPA chosen results to be inside the entry corridor.

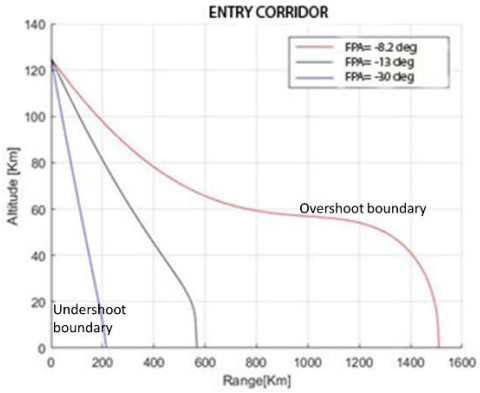


Figure 15: Entry corridor and final trajectory reported as altitude/range trend

In addition to the graph above, the nominal trajectory in Mars-centered inertial frame is reported in the Figure 16.

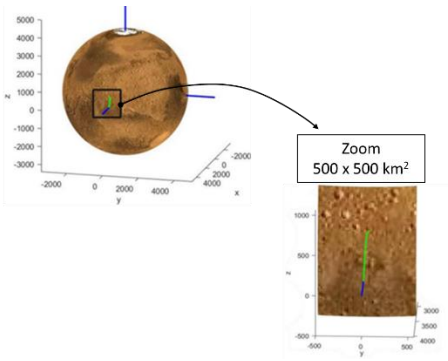


Figure 16: Trajectory in Mars centered inertial frame

In the Figure 17, the trends of g-load, heat flux and dynamic pressure are reported. In the graph, the changes of configurations are identified in discontinuity of the trends (in particular, at16 km and 13.3 km).

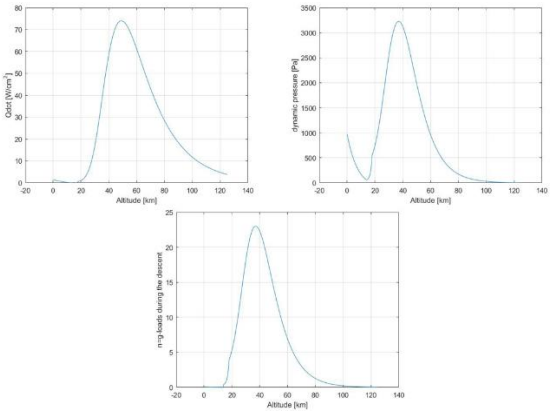

Figure 17: gload, heat flux and dynamic pressure trend

Finally, in the following table, the data regarding the penetration depth and g load after impact are reported.

Table 5: Penetration depth, gload and impact velocity

| | |
|---|---|
| Impact velocity | 353.5 m/s |
| g-load | 9088.2 g |
| Penetration depth | 1.9 m |

As can be seen from the value of g-load, it is less then 24000g that is the value reached by SPS of ASTRIUM during the impact test. In addition, this value can be compared with the typical g-load due to impact for a penetrator that is about 5000÷10000g. In fact, as discussed in [17], the maximum g-load for the 15kg-penetrator with 340m/s of impact speed is about 6000 g.

In nature the energy, after an impact, is dissipated as heat, elastic deformation and other but in preliminary way considering the worst case is a good assumption. Regarding the trajectory (Figure 16), since the heading angle is equal to 0, the entry module must go toward north. In addition, since the 3D trajectory is in fixed-planetocentric Frame, in a certain altitude the probes must be integral with the planet during its rotation, so the last part of the trajectory is curved to the east.

Since all data are known, the updated of design reference mission of SALUS-1 are reported in the Figure 18.

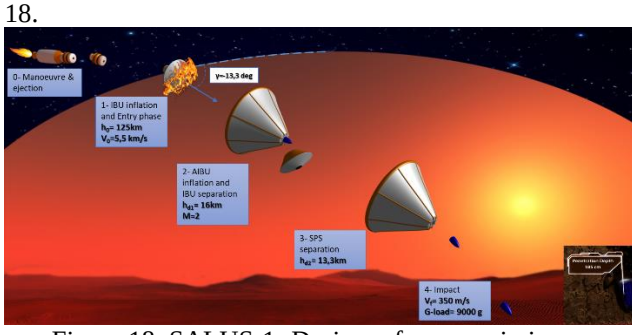


Figure 18: SALUS-1- Design reference mission

## 5. Conclusions

The goal of this study is to describe in detail the design methodology for EDL system during the preliminary phase of the design.

This methodology has been applied on a non-conventional spacecraft to demonstrate the feasibility of the EDI phase for the mission SALUS-1 from the results obtained by simulation tool.

To complete these analyses, more improvement of the code and then, more iterations of the design should be done.

In the future, the simulator tool could be upgraded implementing the 6-DoF dynamics in order to study the attitude control of the entry vehicle. This is very important because the attitude control implementation and a study about the dynamic stability of all configurations could optimize the EDI manoeuvres increasing the feasibility of the mission.

In order to obtain a more accurate result, the planetary model could be improved considering a geodetic system and so a great approximation of the gravity field respect to the latitude and longitude.

Regarding the terminal ballistic, as it has been discussed in the [15], the penetration depth could be obtained thanks to FEA (Finite Element Analysis). From this analysis, the accurate energy impact and other energy could be defined in order to evaluate the g-load due to the impact.

## References

[1] J. Schoolcraft, A. T. Klesh, and T. Werne, "MarCO: Interplanetary Mission Development On a CubeSat Scale," *SpaceOps 2016 Conf.*, no. May 2016, pp. 1–8, 2016, doi: 10.2514/6.2016-2491.

[2] S. Corpino and F. Stesina, "Inspection of the cis-lunar station using multi-purpose autonomous Cubesats," *Acta Astronaut.*, vol. 175, pp. 591–605, 2020.

[3] M. A. Viscio *et al.*, "Interplanetary cubesats mission to earth-sun libration point for space weather evaluations," *Proc. Int. Astronaut. Congr. IAC*, vol. 2, pp. 1324–1332, 2013.

[4] C. Conigliaro, D. Calvi, L. Franchi, F. Stesina, and S. Corpino, "Design and analysis of an innovative cubesat thermal control system for biological experiment in lunar environment," in *Proceedings of the International Astronautical Congress, IAC*, 2018, vol. 2018-Octob.

[5] H. Kalita and J. Thangavelautham, "Lunar CubeSat Lander to Explore Mare Tranquilitatis pit," no. January, pp. 1–12, 2020, doi: 10.2514/6.2020-2163.

[6] F. Nichele, S. Corpino, and S. Seager, "Three scenarios for valuable planetary science missions on mars: Next generation of CubeSats to support space exploration," *Proc. Int. Astronaut. Congr. IAC*, vol. 6, pp. 4121–4135, 2014.

[7] A. M. Harri *et al.*, "The MetNet vehicle: A lander to deploy environmental stations for local and global investigations of Mars," *Geosci. Instrumentation, Methods Data Syst.*, vol. 6, no. 1, pp. 103–124, 2017, doi: 10.5194/gi-6-103-2017.

[8] ESA, *CDF Study Report: CLEO/P (assessment of a Europa Penetrator Mission)*. 2015.

[9] NASA, "Mars Exploration Program Analysis Group (MEPAG)." https://mepag.jpl.nasa.gov/reports.cfm?expand=science.

[10] A. Ball;, J. Garry;, R. Lorenz;, and V. Kerzhanovich, *Planetary Landers and Entry*

*Probes*. 2007.

[11] K. Sutton and R. Graves, "A general stagnation-point convective-heating equation for arbitrary gas mixtures," 1971. [Online]. Available: https://strives-uploads-prod.s3.us-gov-west-1.amazonaws.com/19720003329/19720003329.pdf?AWSAccessKeyId=AKIASEVSKC45ZTTM42XZ&Expires=1601653960&Signature=jXYDuRqRQP2FSIToD9N72NefYkY%3D.

[12] R. C. Wingrove, "Survey of atmosphere re-entry guidance and control methods," *AIAA J.*, vol. 1, no. 9, pp. 2019–2029, 1963, doi: 10.2514/3.1987.

[13] M. Afzal, "Design and analysis of vehicle and guidance concept for interplanetary return mission."

[14] NASA, "Mars Atmosphere model." https://www.grc.nasa.gov/WWW/K-12/airplane/atmosmrm.html#:~:text=Mars Atmosphere Model - Metric Units&text=The Martian atmosphere is an,to the edge of space.&text=Thus%2C the gas temperature is,decreases as we increase altitude.

[15] N. KılıÇ, B. Ekici, and S. Hartomacıoğlu, "Determination of penetration depth at high velocity impact using finite element method and artificial neural network tools," *Def. Technol.*, vol. 11, no. 2, pp. 110–122, 2015, doi: 10.1016/j.dt.2014.12.001.

[16] C. W. Young, "Penetration equation." 1997.

[17] S. Vijendran, J. Fielding, J. Köhler, R. Gowen, and P. Church, "PENETRATOR FOR THE JUPITER GANYMEDE ORBITER MISSION," 2010.